2021 American Control Conference (ACC)
New Orleans, USA, May 25-28, 2021

Robust Vehicle Lane Keeping Control with Networked Proactive Adaptation

Hunmin Kim†, Wenbin Wan†, Naira Hovakimyan†, Lui Sha‡, and Petros Voulgaris*

***Abstract*— Road condition is an important environmental factor for autonomous vehicle control. A dramatic change in the road condition from the nominal status is a source of uncertainty that can lead to a system failure. Once the vehicle encounters an uncertain environment, such as hitting an ice patch, it is too late to reduce the speed, and the vehicle can lose control. To cope with unforeseen uncertainties in advance, we study a proactive robust adaptive control architecture for autonomous vehicles' lane-keeping control problems. The data center generates a prior environmental uncertainty estimate by combining weather forecasts and measurements from anonymous vehicles through a spatio-temporal filter. The prior estimate contributes to designing a robust heading controller and nominal longitudinal velocity for proactive adaptation to each new condition. The control parameters are updated based on posterior information fusion with on-board measurements.**

I. Introduction

Self-driving cars have been one of the most active research areas in the lat few decades [1]. The autonomous vehicles are safety-critical systems operating in dynamic environments. Their controllers should cope with environmental changes robustly. The current paper is motivated by safely controlling the car when hitting an ice patch unexpectedly. Low speed can reduce the risk of skidding, but it may be too late to reduce the speed when hitting an ice patch. The vehicle should slow down in advance and update the controller for the new operating condition.

Model predictive control (MPC) approach has recently proven its effectiveness for robust and optimal control of vehicle dynamics [2], [3]. However, the risk of skidding under dramatic changes of road conditions is not eliminated, because MPC's prediction quality is determined by limited prior knowledge. It starts to adapt to or learn an uncertain environment after encountering it and taking this information into account. Communication network-enabled controllers can address a part of the problem by incorporating environmental information shared from preceding vehicles [4], [5]. Motivated by those papers, the current paper leverages vehicle-to-cloud (V2C) communication for a proactive robust adaptive control architecture for lateral dynamics, by systematically combining environmental measurements from anonymous vehicles and weather forecast.

A. Our Contribution

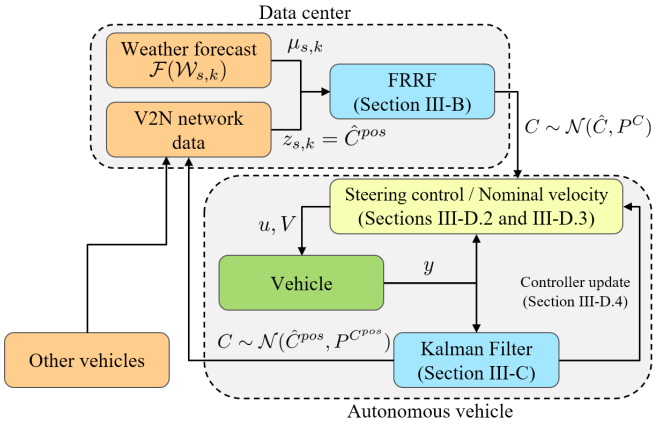

Fig. 1: (Overall architecture) The data center provides a prior estimate. Controller and velocity are proactively designed based on it for each area of the road.

The current paper proposes a novel proactive robust adaptive control architecture for autonomous vehicles to operate with guaranteed performance in various environmental conditions. Figure 1 illustrates the overall system architecture. The prior of the cornering stiffness for different areas is estimated by a newly developed fixed rank resilient filter (FRRF) that fuses information from the weather forecast and vehicle network data. The $\mathcal{L}_1$ adaptive heading controller and nominal longitudinal velocity are designed proactively for each area based on the prior distribution of the cornering stiffness. The proactive adaptation will reduce long-term and large scale uncertainty, while the $\mathcal{L}_1$ adaptive controller deals with fine-scale uncertainty. Then, based on the posterior distribution of the cornering stiffness obtained from the on-board measurements, the control parameters are updated. The full version of the current paper can be found in [6], which contains details of the derivation and the properties of FRRF.

B. Related work

The majority of existing communication network-enabled controllers rely on short-range vehicle-to-vehicle communication between limited connected vehicles for longitudinal control (platooning). In particular, [4] designs a disturbance observer-based controller for platooning. The observer estimates the road slope and shares this information with the following platoons to help them reduce the fuel consumption. Reference [5] studies the optimal trade-off between air drag

This work has been supported by the National Science Foundation (CNS-1932529) and UIUC STII-21-06.

†Hunmin Kim, Wenbin Wan, and Naira Hovakimyan are with the Department of Mechanical Science and Engineering, University of Illinois at Urbana-Champaign, USA. {hunmin, wenbinw2, nhovakim}@illinois.edu

‡Lui Sha is with the Department of Computer Science, University of Illinois at Urbana-Champaign, USA. lrs@illinois.edu

*Petros Voulgaris is with the Department of Mechanical Engineering, University of Nevada, Reno, USA. pvoulgaris@unr.edu

reduction and powertrain energy losses, exploiting a preview from the preceding vehicle. Other network-enabled applications include collision avoidance between vehicles [7], [8].

Our control strategy relies on the $\mathcal{L}_1$ adaptive control [9], [10], which can promptly compensate for unmodeled uncertainties within the filter bandwidth while guaranteeing transient and steady-state performance. Due to such merit, the $\mathcal{L}_1$ adaptive controller has been used as an ancillary controller to ensure that the real system performs as the nominal system. The $\mathcal{L}_1$ adaptive controller has been integrated with model predictive path integral control [11] and with contraction control [12], [13]. The $\mathcal{L}_1$ adaptive controller has been applied to the vehicle lateral dynamics that demonstrates successful compensation for unmodeled uncertainty, such as parametric uncertainty, wind gust, and disturbances of various natures [14].

The prior estimation of the cornering stiffness is a spatio-temporal data fusion problem because the road information contains its attribute as well as spatial and temporal information. Spatio-temporal modeling and filtering have been widely used in environmental process estimation [15], [16]. In particular, the spatio-temporal fixed rank filter in [16] improves the computational efficiency using spatio-temporal models defined on a fixed dimensional space. The current paper extends the spatio-temporal fixed rank filter to capture model uncertainty and (unmodeled) biased noises.

II. Vehicle Lateral Dynamics and Problem Statement

The bicycle model is a simplified vehicle model that has been widely used and has been proven as a good approximation [2], [3], [17]. The variables p^y, p^ψ, V, and δ denote the lateral position, yaw angle, (longitudinal) velocity, and front steering angle, respectively. Parameters C_f, C_r, m, I_z, ℓ_f, and ℓ_r are the front/rear cornering stiffness, mass, yaw moment of inertia, and distance of front/rear tire from the center of gravity, respectively. Given a constant velocity V, the desired lateral position $p^{y,des}$ (center of the lane) and the desired yaw angle $p^{\psi,des}$, the error dynamics of the bicycle model take the form ((2.45) in [17]):

$$\dot{x} = A(V, C_f, C_r)x + b(C_f)u + g(V, C_f, C_r)\dot{p}^{\psi,des}, \quad (1)$$

where $x = [x_1, \dot{x}_1, x_2, \dot{x}_2]^\top$, $x_1 \triangleq p^y - p^{y,des}$ and $x_2 \triangleq p^\psi - p^{\psi,des}$ are the error states, and input $u = \delta$ is the heading. The rate of the desired yaw angle is found by $\dot{p}^{\psi,des} = \frac{V}{R}$, where R is the radius of the road. The system matrices are

$$A(V, C_f, C_r) = \begin{bmatrix} 0 & 1 & 0 & 0 \\ 0 & -2\frac{C_f+C_r}{mV} & 2\frac{C_f+C_r}{m} & 2\frac{-C_f\ell_f+C_r\ell_r}{mV} \\ 0 & 0 & 0 & 1 \\ 0 & -2\frac{C_f\ell_f-C_r\ell_r}{I_zV} & 2\frac{C_f\ell_f-C_r\ell_r}{I_z} & -2\frac{C_f\ell_f^2+C_r\ell_r^2}{I_zV} \end{bmatrix}$$

$b(C_f) = b^o$, $g(V, C_f, C_r) = [0, -2\frac{C_f\ell_f-C_r\ell_r}{mV} - V, 0, -2\frac{C_f\ell_f^2+C_r\ell_r^2}{I_zV}]^\top$. It is worth emphasizing that matrices A and g depend on velocity V, and that the matrices A, b, and g depend on cornering stiffnesses C_f and C_r. For notational simplicity, we express them as $A(V)$, b, and $g(V)$, when their dependency on cornering stiffnesses does not need to be emphasized.

The cornering stiffness C_f (and C_r) is the coefficient related to the lateral force F_f and sliding angle β, where it has a linear relation $F_f = C_f\beta$ for small β. This parameter is closely related to the road friction. In this paper, the cornering stiffnesses C_f and C_r are assumed to be unknown, and we can estimate them using the following information.

Information 2.1: i) weather forecast, ii) vehicle network data (anonymous vehicles' cornering stiffness estimates), iii) on board measurement (GPS, IMU).

We formulate the problem of interest as follows.

Problem 2.1: Given Information 2.1, the problem is to develop a robust control architecture that stabilizes the error dynamics (1) of the vehicle operating under different environmental conditions through controlling the heading $u = \delta$ and longitudinal velocity V.

III. Proactive Robust Adaptive Control

A. Overall architecture

Consider the architecture in Figure 1 to address Problem 2.1. The data center acquires the first two pieces in Information 2.1 about C_f and C_r, which are fused to estimate the prior of cornering stiffness for each area by FRRF algorithm in Section III-B. This will provide a heatmap of the cornering stiffness for multiple areas. Given the cornering stiffness's prior distribution, we pre-design a robust controller and a constant longitudinal velocity for each area of interest. The design procedure for the $\mathcal{L}_1$ adaptive control and the velocity design for a single area is outlined in Sections III-D.2 and III-D.3, and this procedure can be repeated for other areas. The on-board measurement and prior estimate are fused to produce a posterior cornering stiffness estimate of the current area in Section III-C. The posterior information is then used to update the control parameters presented in Section III-D.4.

Remark 3.1: We must design the velocity before encountering an uncertain environment. Since the system matrices depend on the velocity, the velocity and controller are simultaneously designed based on the prior distribution of the cornering stiffness rather than the posterior distribution.

B. Prior estimation: Spatio-temporal fixed rank resilient filtering

The information about the cornering stiffness from weather forecast and anonymous vehicles contains its attribute as well as spatial and temporal information. The estimation of the cornering stiffness can be formulated as a spatio-temporal data fusion problem. We propose to extend the spatio-temporal fixed rank filter [16] to a fixed rank resilient filter (FRRF) such that the filter captures model uncertainty and (unmodeled) biased noises. Assume the cornering stiffness C_f (or C_r) follows a spatio-temporal process $\{q_{s,k} : s \in D, k \in \{1, 2, \cdots, n_D\}\}$, where $q_{s,k} \in \mathbb{R}$, and D is the index set of spatial domains (or area), and

k is the discrete-time index. Domain D could be finite, or countably infinite. Now consider the spatio-temporal mixed effect model [16], [18]:

$$\begin{aligned} q_{s,k} &= \mu_{s,k} + S_{s,k}\eta_k + \xi_{s,k} \\ z_k &= [z_{s_{1_k},k}, z_{s_{2_k},k}, \cdots, z_{s_{n_k},k}]^\top \\ z_{s,k} &= q_{s,k} + \epsilon_{s,k}, \end{aligned} \tag{2}$$

where $z_{s,k} \in \mathbb{R}$ is the output of area s at time k and is subject to measurement noise $\epsilon_{s,k}$. At time k, we observe n_k sensor outputs, and the collection of outputs is denoted by $z_k \in \mathbb{R}^{n_k}$. The collection of measured area indices is denoted by $O_k = \{s_{1_k}, s_{2_k}, \cdots, s_{n_k}\} \subseteq D$. Anonymous vehicles estimate the cornering stiffness of the presence area and send the estimates to the center through V2C communication. This vehicle network data represents the output z_k.

Consider the first equation in (2). The first term $\mu_{s,k} \in \mathbb{R}$ is a known time-varying value that models large scale variation. For the cornering stiffness estimation problem, we assume $\mu_{s,k}$ is a function of weather forecast $\mathcal{W}_{s,k}$ (including temperature, precipitation, humidity, wind, and more), i.e., $\mu_{s,k} = \mathcal{F}(\mathcal{W}_{s,k})$. The mapping function $\mathcal{F}(\cdot)$ can be found by standard learning/regression algorithms (e.g., Gaussian process regression, neural network, basis function regression) by using historical input-output data $\langle \mathcal{W}_{s,k}, C_{f,k} \rangle$. In the current paper, we assume the function $\mathcal{F}$ is given.

The second term $S_{s,k}\eta_k$ captures a smooth small scale variation that correlates the spatial relation between different areas by the finite n_η-dimensional spatial basis $S_{s,k}$. Matrix $S_{s,k}$ is known, but the state variable $\eta_k \in \mathbb{R}^{n_\eta}$ is unknown. The third term $\xi_{s,k} \in \mathbb{R}$ presents time-dependent fine-scale variation that captures the nugget effect. The state variable η_k is supposed to evolve according to the following dynamic equation: $\eta_{k+1} = H_k\eta_k + G_k d_k + \zeta_k$, where H_k and G_k are known matrices. The first term $H_k\eta_k$ captures temporal correlation, and the row of H_k can be chosen to be zeros, if the corresponding component η_{k+1} does not change dynamically. The second term $G_k d_k$ denotes a biased noise and model uncertainty, where $d_k \in \mathbb{R}^{n_d}$ is unknown, and it can be seen as an unknown input. This term is absent in [16], [18]. The last term $\zeta_k \in \mathbb{R}^{n_\eta}$ represents a fine-scale variation of hidden state η_k. All noises $\epsilon_{s,k}$, $\xi_{s,k}$, ζ_k are independent zero-mean Gaussian with covariance $P^\epsilon_{s,k}$, $P^\xi_{s,k}$, and P^ζ_k, respectively.

Our interest is to recursively estimate the hidden state $q_{s_*,k}$ for the query area $s_* \in D$. Denote μ_k, S_k, ϵ_k, ξ_k the collection of the corresponding values for all $s \in O_k$ and define $P^\epsilon_k = diag(P^\epsilon_{s,k})$ and $P^\xi_k = diag(P^\xi_{s,k})$ for all $s \in O_k$ for simplicity. The matrix $E_k \in \{0,1\}^{n_k \times n_D}$ denotes the output matrix having 1 for $(1, s_{1_k}), \cdots, (n_k, s_{n_k})$ elements, and 0 for the others. Let $\hat{v}_k$, $\tilde{v}_k \triangleq v_k - \hat{v}_k$, and $P^v_k \triangleq \mathbb{E}[(v_k - \hat{v}_k)(v_k - \hat{v}_k)^\top]$ denote the estimate, estimation error, and estimation covariance of a variable v at time k.

The estimate $\hat{q}_{s_*,k}$ represents an estimate of cornering stiffness C_f (or C_r). Appendices VI-A, and VI-B in [6] present detailed derivation and properties of FRRF. The derivation of the algorithm is motivated by fixed rank filtering [16] and unknown input and state estimation algorithms [19], and, thus, they also share similar properties.

The summary of the proposed algorithm is shown below. Given the output $z_{s,k}$ and the previous estimate $\hat{\eta}_{k-1}$, the unknown variable η_k is estimated by rejecting the unmodeled uncertainty d_k. The variable $q_{s,k}$ in (2) is estimated from $\hat{\eta}_k$ compensating for fine-scale variation $\xi_{s,k}$ by its estimate $\hat{\xi}_{s,k}$.

Recursive prediction:

$$\begin{aligned} &\hat{\eta}_{k|k-1} = H_{k-1}\hat{\eta}_{k-1} + G_{k-1}M_k(z_k - \mu_k - S_k H_{k-1}\hat{\eta}_{k-1}) \\ &P^\eta_{k|k-1} = (\mathbb{I} - G_{k-1}M_k S_k)H_{k-1}P^\eta_{k-1}H^\top_{k-1}(\mathbb{I} \\ &- G_{k-1}M_k S_k)^\top + G_{k-1}M_k(P^\epsilon_k + E_k P^\xi_k E_k^\top)M_k^\top G^\top_{k-1} \\ &+ (\mathbb{I} - G_{k-1}M_k S_k)P^\zeta_{k-1}(\mathbb{I} - G_{k-1}M_k S_k)^\top, \end{aligned}$$

where $M_k = (G^\top_{k-1}S_k^\top R_k^{-1} S_k G_{k-1})^\dagger G^\top_{k-1} S_k^\top R_k^{-1}$, and $R_k = S_k(H_{k-1}P^\eta_{k-1}H^\top_{k-1} + P^\zeta_{k-1})S_k^\top + P^\epsilon_k + E_k P^\xi_k E_k^\top$.

Recursive estimation:

$$\begin{aligned} &\hat{\eta}_k = \hat{\eta}_{k|k-1} + K_k(z_k - \mu_k - S_k\hat{\eta}_{k|k-1}) \\ &P^\eta_k = (\mathbb{I} - K_k S_k)P^\eta_{k|k-1}(\mathbb{I} - K_k S_k)^\top + K_k(P^\epsilon_k \\ &\quad + E_k P^\xi_k E_k^\top)K_k^\top + (\mathbb{I} - K_k S_k)M_k(P^\epsilon_k + E_k P^\xi_k E_k^\top)K_k^\top \\ &\quad + K_k(P^\epsilon_k + E_k P^\xi_k E_k^\top)M_k^\top(\mathbb{I} - K_k S_k)^\top, \end{aligned}$$

where $K_k = (P^\eta_{k|k-1}S_k^\top - M_k(P^\epsilon_k + E_k P^\xi_k E_k^\top))\tilde{R}_k^{-1}$, and $\tilde{R}_k = S_k P^\eta_{k|k-1}S_k^\top + (P^\epsilon_k + E_k P^\xi_k E_k^\top) - S_k M_k(P^\epsilon_k + E_k P^\xi_k E_k^\top) - (P^\epsilon_k + E_k P^\xi_k E_k^\top)M_k^\top S_k^\top$.

Estimation of $q_{s_*,k}$:

$$\begin{aligned} &\hat{q}_{s_*,k} = \mu_{s_*,k} + S_{s_*,k}\hat{\eta}_k + \hat{\xi}_{s_*,k} \\ &\hat{\xi}_{s_*,k} = L_{s_*,k}(z_k^{s_*} - \mathbf{1}\mu_{s_*,k} - \mathbf{1}S_{s_*,k}\hat{\eta}_{k|k-1}) \\ &P^q_{s_*,k} = S_{s_*,k}K_k S_k P^\eta_{k|k-1}(S_{s_*,k}K_k S_k)^\top + P^\epsilon_{s_*,k}L_{s_*,k}L^\top_{s_*,k} \\ &+ S_{s_*,k}K_k(P^\epsilon_k + E_k P^\xi_k E_k^\top)(S_{s_*,k}K_k)^\top \\ &+ S_{s_*,k}K_k P^{s,s_*,\epsilon}_k L^\top_{s_*,k} + L^\top_{s_*,k}P^{s_*,s,\epsilon}_k K_k^\top S^\top_{s_*,k} \\ &+ S_{s_*,k}K_k S_k G_{k-1}M_k((P^\epsilon_k + E_k P^\xi_k E_k^\top)K_k^\top S^\top_{s_*,k} \\ &+ P^{s,s_*,\epsilon}_k L^\top_{s_*,k}) + (S_{s_*,k}K_k(P^\epsilon_k + E_k P^\xi_k E_k^\top) \\ &+ L_{s_*,k}P^{s_*,s,\epsilon}_k)(S_{s_*,k}K_k S_k G_{k-1}M_k)^\top, \text{ if } s_* \in O_k \\ &P^q_{s_*,k} = S_{s_*,k}P^\eta_k S^\top_{s_*,k} + P^\xi_{s_*,k}, \text{ otherwise,} \end{aligned}$$

where $z_k^{s_*}$ is the collection of outputs $z_{s,k}$ for $s = s^*$,

$$L_{s_*,k} = \begin{cases} (\mathbf{1}^\top \bar{R}^{-1}_{s_*,k}\mathbf{1})^{-1}\mathbf{1}^\top \bar{R}^{-1}_{s_*,k} & \text{if } s_* \in O_k \\ 0 & \text{otherwise,} \end{cases}$$

and $\bar{R}_{s_*,k} = P^\epsilon_{s_*,k}\mathbb{I} + \mathbf{1}S_{s_*,k}P^\eta_{k|k-1}S^\top_{s_*,k}\mathbf{1}^\top - \mathbf{1}S_{s_*,k}G_{k-1}M_k P^{s,s_*,\epsilon}_k - P^{s_*,s,\epsilon}_k(\mathbf{1}S_{s_*,k}G_{k-1}M_k)^\top$, $P^{s,s_*,\epsilon}_k \triangleq \mathbb{E}[\epsilon_k(\epsilon^{s_*}_k)^\top]$.

C. Posterior estimation: Real-time local information fusion

The posterior estimation of cornering stiffness utilizes the standard Kalman filtering on the bicycle model [20], [21], taking three outputs: 1) GPS measurement, 2) IMU measurement, and 3) prior estimate obtained in Section III-B. This method will use the prior estimate as one of the (less frequently measured) outputs. GPS and IMU sensors that are already implemented or easy to be installed are enough to estimate the cornering stiffness [21].

D. $\mathcal{L}_1$ adaptive control with proactive velocity design

We implement the $\mathcal{L}_1$ adaptive controller [10] for the lane-keeping control, which provides rapid disturbance compensation within the filter bandwidth while guaranteeing transient and steady-state performance. Different controllers should be designed for different areas, because the prior distribution of the cornering stiffness varies by location. The current section provides a controller design for one area, and the same design procedure can be repeated for all other areas of interest.

Section III-D.1 introduces the $\mathcal{L}_1$ adaptive controller on its nominal system [10]. Section III-D.2 discusses how to transform the error dynamics (1) to the nominal system for the $\mathcal{L}_1$ adaptive controller using the prior distribution of the cornering stiffness. In particular, the nominal system model for the $\mathcal{L}_1$ adaptive controller is determined by the mean of the prior distribution obtained in Section III-B. Section III-D.3 provides the design procedure for the $\mathcal{L}_1$ adaptive controller and the velocity for the error dynamics.

1) $\mathcal{L}_1$ adaptive controller: Consider the following system:

$$\begin{aligned} \dot{x}(t) &= A_m x(t) + b_m(w u_{ad}(t) + \theta^\top x(t) + \sigma(t)) \\ y(t) &= c^\top x(t) \qquad x(0) = x_0, \end{aligned} \tag{3}$$

where A_m, b_m, and c are known system matrices/vectors, and A_m is Hurwitz. Parameter $w \in \mathbb{R}$ is the unknown input gain, and the state-dependent uncertainty is represented by $b_m\theta^\top x(t)$, where θ is an unknown vector. The uncertain parameters satisfy Assumption 3.1. The signal $\sigma(t)$ is the time-varying external disturbance that satisfies Assumption 3.2.

Assumption 3.1: We have $w \in \Omega = [w_l, w_u]$, and $\theta \in \Theta$, where the bound $[w_l, w_u]$ and convex set Θ are known.

Assumption 3.2: The disturbance signal $\sigma(t)$ is continuously differentiable, and the signal and its derivative are uniformly bounded, i.e., $|\sigma(t)| \le \Delta$, and $|\dot{\sigma}(t)| \le d_\sigma < \infty$ for $\forall t \ge 0$, where the bounds Δ and d_σ are known.

The control input $u_{ad}(t)$ is an adaptive controller that consists of state predictor, adaptation law, and low-pass filter. In what follows, we describe the $\mathcal{L}_1$ adaptive controller.

State predictor: The state predictor is given by

$$\begin{aligned} \dot{\hat{x}}(t) &= A_m\hat{x}(t) + b_m(\hat{w}(t)u_{ad}(t) + \hat{\theta}^\top x(t) + \hat{\sigma}(t)) \\ \hat{y}(t) &= c^\top\hat{x}(t) \qquad \hat{x}(0) = \hat{x}_0. \end{aligned}$$

Adaptation laws: The adaptation laws are given by:

$$\begin{aligned} \dot{\hat{w}}(t) &= \Gamma Proj(\hat{w}(t), -\tilde{x}^\top(t)Pb_m u_{ad}(t)) \qquad \hat{w}(0) = \hat{w}_0 \\ \dot{\hat{\theta}}(t) &= \Gamma Proj(\hat{\theta}(t), -\tilde{x}^\top(t)Pb_m x(t)) \qquad \hat{\theta}(0) = \hat{\theta}_0 \\ \dot{\hat{\sigma}}(t) &= \Gamma Proj(\hat{\sigma}(t), -\tilde{x}^\top(t)Pb_m) \qquad \hat{\sigma}(0) = \hat{\sigma}_0, \end{aligned}$$

where $\tilde{x}(t) = \hat{x}(t) - x(t)$ is the prediction error, and $\Gamma > 0$ is an adaptation gain, $Proj(\cdot,\cdot)$ is the projection operator defined in Definition B.3 in [10]. The projection operator guarantees that each estimate remains in its desired domain. Matrix P is a symmetric positive definite matrix, solving the algebraic Lyapunov equation $A_mP + PA_m^\top = -Q$ for a given symmetric positive definite matrix Q.

Control law: The adaptive control input is designed by

$$u_{ad}(s) = -kD(s)(\hat{\eta}(s) - k_g r(s)),$$

where $\hat{\eta}(t) = \hat{w}(t)u_{ad}(t) + \hat{\theta}^\top(t)x(t) + \hat{\sigma}(t)$ and $k_g = -1/(c^\top A_m^{-1}b_m)$, and $k > 0$ is a constant. The signal $r(s)$ is the Laplace transform of the reference signal, and $D(s)$ is a strictly proper transfer function that leads to a strictly proper stable low-pass filter $C(s) = \frac{wkD(s)}{1+wkD(s)}$ with $C(0) = 1$. Low-pass filter $C(s)$ trades off the performance against robustness, i.e., increasing bandwidth of the filter results in low time-delay margin, with improved tracking performance. We choose $D(s) = 1/s$ in this paper. We need to choose the controller such that the $\mathcal{L}_1$-norm condition is satisfied: $\|G(s)\|_{\mathcal{L}_1}L < 1$, where $G(s) = H(s)(1 - C(s))$, $H(s) = (s\mathbb{I} - A_m)^{-1}b_m$, and $L = \max_{\theta\in\Theta}\|\theta\|_1$. Since θ is constant and $D(s) = 1/s$, the $\mathcal{L}_1$-norm condition reduces to

$$A_g = \begin{bmatrix} A_m + b_m\theta^\top & b_m w \\ -k\theta^\top & -kw \end{bmatrix} \tag{4}$$

being Hurwitz for all $\theta \in \Theta$ and $w \in \Omega_0$.

2) System transformation and bounds of uncertainties: The system (1) is uncertain, where the system matrices $A(V, C_f, C_r)$ and $b(C_f)$ depend on unknown cornering stiffness C_f and C_r, while A_m and b_m in (3) are known. We will use the mean values $\hat{C}_f = \hat{q}_{s_*,k}$ (and $\hat{C}_r = \hat{q}'_{s_*,k}$) of the prior distribution to construct nominal system matrices, i.e., with $u = u_m + u_{ad}$ and $u_m = -Kx$, $A_m = A(V, \hat{C}_f, \hat{C}_r) - b(\hat{C}_f)K$ and $b_m = b(\hat{C}_f)$. The bound of uncertainties can be found by a 95% confidence interval of the cornering stiffness.

3) $\mathcal{L}_1$ adaptive controller and nominal velocity design: The $\mathcal{L}_1$ adaptive controller guarantees transient and steady-state performance with respect to the reference system and design system. The reference system is the non-adaptive version of the $\mathcal{L}_1$ adaptive controller. The design system is an ideal system that does not depend on the uncertainties. According to Theorem 2.2.2 in [10], the performance of the system can be arbitrary close to the reference system ($x_{ref}(t)$ and $u_{ref}(t)$) by increasing the adaptation gain Γ without sacrificing robustness. Lemma 2.1.4 in [10] analyzes the error between the reference system and the design system ($\|x_{ref} - x_{des}\|_{\mathcal{L}_\infty}$ and $\|u_{ref} - u_{des}\|_{\mathcal{L}_\infty}$), where its upper bound is proportional to $\|G(s)\|_{\mathcal{L}_1}$. The term $\|G(s)\|_{\mathcal{L}_1}$ can be close to zero by arbitrarily increasing the filter bandwidth k. However, this performance improvement trades off with the robustness. The time-delay margin decreases to zero, as k increases to infinity. Therefore, we need to design k_m, $C(s)$, and V balancing the performance and robustness optimally.

The matrix $A_m(V)$ must be Hurwitz, but it depends both on gain k_m and velocity V. To relax this complexity, we propose to use the common Lyapunov function approach. We first design control gains k_m and P such that $A_m(V)$ is Hurwitz for any velocity $V \in [V_{\min}, V_{\max}]$, where $V_{\min}$ and $V_{\max}$ are the minimum and maximum velocity of the area. Upon that, we choose the velocity V and filter $C(s)$ simultaneously through an optimization problem.

Given $\hat{C}_f$ and $\hat{C}_r$, we should choose constant vector k_m and symmetric positive definite matrix P such that $A_m(V)P + PA_m^\top(V) < 0$ holds for all $V_{\min} \le V \le V_{\max}$.

We can choose the filter gain k and the velocity V balancing the performance and robustness. The performance

is characterized by $\|G(s)\|_{\mathcal{L}_1}$ as in [22]. The robustness is characterized by a lower bound of k, which prevents the time-delay margin from converging to zero. The optimization problem can be formulated by

$$\max_{k,V\in[V_{\min},V_{\max}]} V$$
$$s.t.\ k \le \bar{k},\ \|G(s)\|_{\mathcal{L}_1} \le \lambda_{gp},\ \text{for}\ \forall w \in \Omega,$$

where $\bar{k} > 0$ and $\lambda_{gp} < \frac{1}{L}$. Recall that $G(s) = H(s)(1 - C(s))$. Given λ_{gp}, one could find the performance bounds of $\|x_{ref} - x_{des}\|_{\mathcal{L}_\infty}$ and $\|u_{ref} - u_{des}\|_{\mathcal{L}_\infty}$ in Lemma 7 in [9].

4) Real-time controller update: It is critically important to ensure that the matrices A_m and A_g are Hurwitz for all possible uncertainties. Given the posterior distribution $\mathcal{N}(\hat{C}_f^{pos}, P^{C_f^{pos}})$ (or $\mathcal{N}(\hat{C}_r^{pos}, P^{C_r^{pos}})$ for rear cornering stiffness) from Kalman filter in Section III-C, we can construct the 95% confidence interval of the posterior distribution of C_f and C_r. We check online whether $A_g(V)$ in (4) is Hurwitz for the new set of uncertainties. If it does not hold, we update k in real-time such that $A_g(V)$ is Hurwitz: $k = \arg\min_k |k - k_*|$, s.t. $k \le \bar{k}$, $A_g(V)$ being Hurwitz, where k_* is the current gain. It is worth noting that A_m does not need to be re-tuned, because it depends only on $\hat{C}_f$ and $\hat{C}_r$, and not on the bounds of uncertainties. Furthermore, we design it to be Hurwitz for the entire possible velocity range.

IV. Simulation

The current section demonstrates the performance of the proposed control architecture. System and control parameters can be found in [6]. Section IV-A presents the resilient estimation performance of FRRF in the presence of (biased) unmodeled uncertainty. Based on the prior estimate, we design the $\mathcal{L}_1$ adaptive controller for the areas of interest and illustrate the lane keeping performance in Section IV-B. All values are in standard SI units; m (meter) for ℓ_f, ℓ_r, R, and x_1; rad for δ and x_2; m/s for V; N/rad for C_f and C_r; kg for m; $kg \cdot m^2$ for I_z.

A. Prior estimation by FRRF

We consider the square area that is divided into 25 identical small squares, i.e., $n_D = 25$. The ground truth cornering stiffness holds $C_f = C_r$ for all the areas, although this information is unknown to the control authority. Given the initial condition $\hat{\eta}_0 = \mathbf{0}$ with covariance $P_0^\eta = 1000\mathbb{I}$, we conduct FRRF algorithm in Section III-B, and present the simulation results in Figs 2 and 3. For each time k, FRRF generates a heat map for the cornering stiffness. Figure 2 presents a series of heat maps produced by the FRRF algorithm, where the color represents the mean value $\hat{q}_{s,k}$ of the corresponding area s.

Figure 3 compares the tracking errors when the outputs are sparsely measured (as a Poisson with $\lambda = 20$) and are fully measured at areas 1 and 2. Areas 1 and 2 are the left bottom corner and its right cell, respectively. The estimation errors for all areas remain in their noise level. FRRF algorithm estimates the ground truth cornering stiffness resiliently, where the errors do not depend on the presence of d_k, as shown in

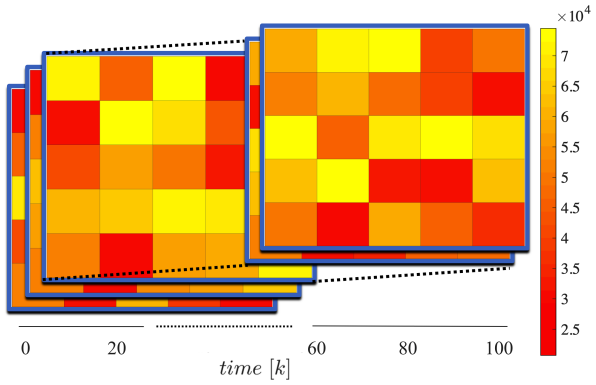

Fig. 2: Prior estimation heatmap. The color represents the mean value of the estimate in the corresponding area.

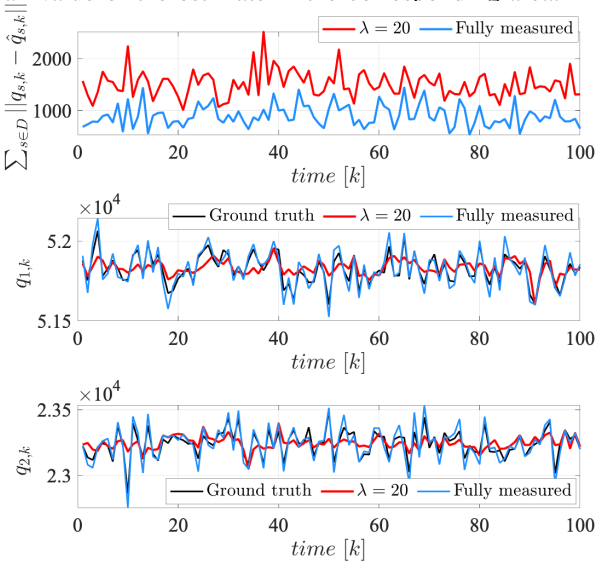

Fig. 3: Prior estimation performance; (top) total estimation error; (middle, bottom) ground truth cornering stiffness and estimates with the full measurement and spares measurement at areas 1 and 2.

the first subfigure. FRRF with the full measurement exhibits an improved tracking performance of fine-scale variation a lot than that with the spares measurement, as presented in the second and third subfigures. This is because FRRF with the full measurement successfully reduces the estimation error by compensating for unmodeled uncertainty at each iteration. The average trace norm of variance in the whole area is $tr(P_k^{q,full}) = 1983.7$ with the full measurement and $tr(P_k^{q,\lambda=20}) = 3190.4$ with the spares measurement.

B. Proactive $\mathcal{L}_1$ adaptive control

The current section compares the tracking performance of the proactive $\mathcal{L}_1$ adaptive control and a non-proactive version of it. We refer to [14] to compare the $\mathcal{L}_1$ adaptive controller's performance with that of other types of controllers.

Figure 4 presents the performance of the proactively designed $\mathcal{L}_1$ adaptive controller under the raining condition ($C_{1,f} = C_{1,r} = 51867$). The controller can successfully stabilize the error dynamics under the changing road radius. With a large adaptation gain, the system performance is arbitrarily close to that of the reference system. Figure 5

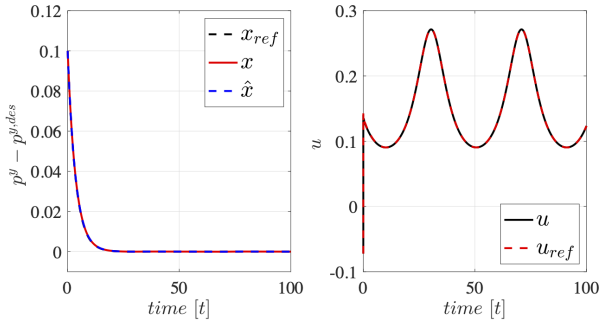

Fig. 4: Raining condition. Error states and control inputs in area 1 ($C_{1,f} = C_{1,r} = 51867$).

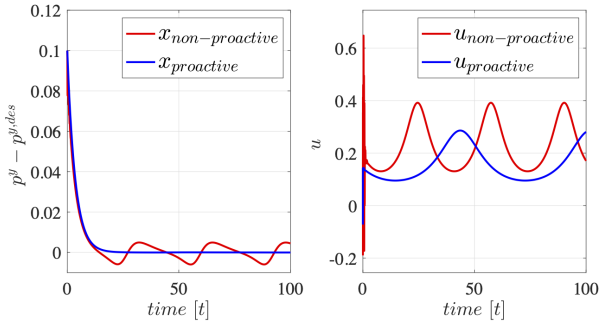

Fig. 5: Snowing condition. Error states and control inputs in area 2 ($C_{2,f} = C_{2,r} = 23214$).

compares the proactive $\mathcal{L}_1$ adaptive controller's tracking performance and the non-proactive version under the snowing condition and changing road radius. The system with the proactive controller does not have performance degradation compared to operating in the raining condition. The non-proactive controller designed for dry road conditions (around $C_f = C_r = 80000$) failed to stabilize the system. As discussed, one could increase k to guarantee stability, but this will harm the robustness. To illustrate the performance difference between the proactive controller and non-proactive controller without increasing k, we consider the controller designed for $C_f = C_r = 60000$. The non-proactive controller could stabilize the error dynamics through compensation of uncertainties, but presents a relatively large error, when the vehicle operates outside of its nominal status.

V. Conclusion

We study a proactive robust adaptive control architecture for autonomous vehicles operating in various environmental conditions. The weather forecast and vehicle network data are used to estimate the unknown cornering stiffness by newly developed FRRF. Given the prior estimate for multiple areas, the $\mathcal{L}_1$ adaptive controller and velocity are designed for each road area, balancing the performance and robustness. The posterior estimate is obtained by combining the prior estimate and the on-board measurement. The controller is updated based on the posterior distribution, if it violates the $\mathcal{L}_1$-norm condition.

References

[1] B. Paden, M. Čáp, S. Z. Yong, D. Yershov, and E. Frazzoli, "A survey of motion planning and control techniques for self-driving urban vehicles," *IEEE Transactions on Intelligent Vehicles*, vol. 1, no. 1, pp. 33–55, 2016.

[2] P. Falcone, F. Borrelli, J. Asgari, H. E. Tseng, and D. Hrovat, "Predictive active steering control for autonomous vehicle systems," *IEEE Transactions on Control Systems Technology*, vol. 15, no. 3, pp. 566–580, 2007.

[3] A. Carvalho, Y. Gao, S. Lefevre, and F. Borrelli, "Stochastic predictive control of autonomous vehicles in uncertain environments," in *12th International Symposium on Advanced Vehicle Control*, pp. 712–719, 2014.

[4] G. Na, G. Park, V. Turri, K. H. Johansson, H. Shim, and Y. Eun, "Disturbance observer approach for fuel-efficient heavy-duty vehicle platooning," *Vehicle System Dynamics*, vol. 58, no. 5, pp. 748–767, 2020.

[5] L. Bertoni, J. Guanetti, M. Basso, M. Masoero, S. Cetinkunt, and F. Borrelli, "An adaptive cruise control for connected energy-saving electric vehicles," *IFAC-PapersOnLine*, vol. 50, no. 1, pp. 2359–2364, 2017.

[6] H. Kim, W. Wan, N. Hovakimyan, and L. Sha, "Robust vehicle lane keeping control with networked proactive adaptation," *arXiv preprint arXiv:2009.12349*, 2020.

[7] S. Biswas, R. Tatchikou, and F. Dion, "Vehicle-to-vehicle wireless communication protocols for enhancing highway traffic safety," *IEEE Communications Magazine*, vol. 44, no. 1, pp. 74–82, 2006.

[8] M. R. Hafner, D. Cunningham, L. Caminiti, and D. Del Vecchio, "Cooperative collision avoidance at intersections: Algorithms and experiments," *IEEE Transactions on Intelligent Transportation Systems*, vol. 14, no. 3, pp. 1162–1175, 2013.

[9] C. Cao and N. Hovakimyan, "Design and analysis of a novel $\mathcal{L}_1$ adaptive control architecture with guaranteed transient performance," *IEEE Transactions on Automatic Control*, vol. 53, no. 2, pp. 586–591, 2008.

[10] N. Hovakimyan and C. Cao, $\mathcal{L}_1$ *Adaptive Control Theory: Guaranteed Robustness with Fast Adaptation*. SIAM, 2010.

[11] J. Pravitra, K. A. Ackerman, C. Cao, N. Hovakimyan, and E. A. Theodorou, "$\mathcal{L}_1$-adaptive MPPI architecture for robust and agile control of multirotors," *IEEE/RSJ International Conference on Intelligent Robots and Systems (IROS)*, pp. 7661–7666, 2020.

[12] A. Lakshmanan, A. Gahlawat, and N. Hovakimyan, "Safe feedback motion planning: A contraction theory and $\mathcal{L}_1$-adaptive control based approach," *IEEE Conference on Decision and Control (CDC)*, pp. 1578–1583, 2020.

[13] A. Gahlawat, A. Lakshmanan, L. Song, A. Patterson, Z. Wu, N. Hovakimyan, and E. Theodorou, "$\mathcal{RL}_1$-$\mathcal{GP}$: Safe simultaneous learning and control," in *3rd Learning for Dynamics and Control (L4DC) Conference*, 2021.

[14] M. M. Shirazi and A. B. Rad, "$\mathcal{L}_1$ adaptive control of vehicle lateral dynamics," *IEEE Transactions on Intelligent Vehicles*, vol. 3, no. 1, pp. 92–101, 2017.

[15] G. Evensen, *Data assimilation: the ensemble Kalman filter*. Springer Science & Business Media, 2009.

[16] N. Cressie, T. Shi, and E. L. Kang, "Fixed rank filtering for spatio-temporal data," *Journal of Computational and Graphical Statistics*, vol. 19, no. 3, pp. 724–745, 2010.

[17] R. Rajamani, *Vehicle dynamics and control*. Springer Science & Business Media, 2011.

[18] H. Nguyen, M. Katzfuss, N. Cressie, and A. Braverman, "Spatio-temporal data fusion for very large remote sensing datasets," *Technometrics*, vol. 56, no. 2, pp. 174–185, 2014.

[19] W. Wan, H. Kim, N. Hovakimyan, and P. G. Voulgaris, "Attack-resilient estimation for linear discrete-time stochastic systems with input and state constraints," in *IEEE Conference on Decision and Control (CDC)*, pp. 5107–5112, 2019.

[20] D. M. Bevly, J. Ryu, and J. C. Gerdes, "Integrating INS sensors with GPS measurements for continuous estimation of vehicle sideslip, roll, and tire cornering stiffness," *IEEE Transactions on Intelligent Transportation Systems*, vol. 7, no. 4, pp. 483–493, 2006.

[21] G. Baffet, A. Charara, and D. Lechner, "Estimation of vehicle sideslip, tire force and wheel cornering stiffness," *Control Engineering Practice*, vol. 17, no. 11, pp. 1255–1264, 2009.

[22] D. Li, N. Hovakimyan, C. Cao, and K. Wise, "Filter design for feedback-loop trade-off of $\mathcal{L}_1$ adaptive controller: A linear matrix inequality approach," in *AIAA Guidance, Navigation and Control Conference and Exhibit*, p. 6280, 2008.